Optimizing Pulsar Timing Arrays Observations for Detection and Characterization of Low-Frequency Gravitational Wave Sources

M. T. LAM^{1, 2}

¹Department of Physics and Astronomy, West Virginia University, White Hall, Morgantown, WV 26506, USA; michael.lam@mail.wvu.edu

²Center for Gravitational Waves and Cosmology, West Virginia University, Chestnut Ridge Research Building, Morgantown, WV 26505

ABSTRACT

Observations of low-frequency gravitational waves will require the highest possible timing precision from an array of the most spin-stable pulsars. We can improve the sensitivity of a pulsar timing array (PTA) to different gravitational-wave sources by observing pulsars with low timing noise over years to decades and distributed across the sky. We discuss observing strategies for a PTA focused on a stochastic gravitational-wave background such as from unresolved supermassive black hole binaries as well as focused on single continuous-wave sources. First we describe the method to calculate a PTA's sensitivity to different gravitational-wave-source classes. We then apply our method to the 45 pulsars presented in the North American Nanohertz Observatory for Gravitational Waves (NANOGrav) 11-year data set. For expected amplitudes of the stochastic background, we find that all pulsars contribute significantly over the timescale of decades; the exception is for very pessimistic values of the stochastic background amplitude. For individual single sources, we find that a number of pulsars contribute to the sensitivity of a given source but that which pulsars contribute are different depending on the source, or versus an all-sky metric. Our results seem robust to the presence of temporally-correlated red noise in pulsar arrival times. It is critical to obtain more robust pulsar-noise parameters as they heavily affect our results. Our results show that it is also imperative to locate and time as many high-precision pulsars as possible, as quickly as possible, to maximize the sensitivity of next-generation PTA detectors.

Keywords: methods: observational — pulsars: general — gravitational waves

1. INTRODUCTION

As the detection of low-frequency gravitational waves (GWs) nears (Taylor et al. 2016), pulsar timing array (PTA) collaborations must begin looking towards the future characterization of the GW sky. As with ground-based detectors, we must begin planning for the next-generation of PTA detectors, one optimized for these observations. The North American Nanohertz Observatory for Gravitational Waves (NANOGrav; McLaughlin 2013) collaboration, one of several efforts worldwide (e.g., Verbiest et al. 2016; Desvignes et al. 2016; Reardon et al. 2016), is currently observing over 70 high-precision millisecond pulsars (MSPs) in its PTA detector for the purpose of low-frequency GW detection from both a stochastic background and from single sources. Without a detection, we have placed constraints on the environments of supermassive black hole binary (SMBHB) mergers, cosmic strings, and inflationary era GWs (Arzoumanian et al. 2015a, 2014, 2018b).

Detector sensitivity depends on the GW signal we wish to observe. A stochastic background requires observations of many MSPs (Siemens et al. 2013; Vigeland & Siemens 2016) whereas the sensitivity to single sources such as from a single binary or merger event requires the highest timing precision from a few of the best-timed MSPs (Ellis et al. 2012). PTA observations require years to decades of a timing baseline to detect nanohertz-regime GWs and there-

fore large amounts of telescope time are required. In theory with enough observing time we could observe enough pulsars with adequate timing-precision to cover both science targets (stochastic background versus single source) but practical limitations apply. NANOGrav currently observes its pulsars on a monthly cadence except for a handful of the highest-precision pulsars which are observed weekly, with the goal of covering both stochastic background and single continuous wave (CW) source characterization. However, the efficacy of the approaches to maximizing GW sensitivity has been unclear so far.

In Lam et al. (2018), we examined pulse arrival-time uncertainty for MSPs as a function of the radio frequencies observed by specific telescopes taking into account a wide variety of effects. The requirements per pulsar vary but large bandwidths covering much of the radio spectrum typically used for high-precision pulsar timing (~GHz) are needed to obtain the best possible arrival-time estimates. In this work, we will consider the time-allocation optimization for various pulsars in the array to maximize overall GW sensitivity. Lee et al. (2012) examined this problem first by considering a simplified PTA and providing the methodology to optimize a specific stochastic-background detection statistic given observing constraints from one or several telescopes.

Here we will develop the methodology for time optimization for the goals of detecting and characterizing both the stochastic background and single CW sources. We apply this

formalism to the 45 pulsars presented in the NANOGrav 11-year data set (NG11; Arzoumanian et al. 2018a), providing specific prescriptions for allocating the observing time per pulsar depending on the two science goals. In §2, we describe the cross-correlation statistic used as our GW sensitivity metric. We apply our formalism to the NG11 pulsars in §3 and describe future directions in §4.

2. THE CROSS-CORRELATION STATISTIC

For the signal-to-noise (S/N) metric that we wish to maximize, we use the cross-correlation statistic derived in Siemens et al. (2013). We first break it into its constituent components for an individual pulsar pair (pulsars labeled with subscripts i, j), given as

$$\rho_{ij} = \left(2T_{ij}\chi_{ij}^2 \int_{f_{\rm L}}^{f_{\rm H}} df \frac{P_g^2(f)}{P_i(f)P_j(f)}\right)^{1/2},\tag{1}$$

where T_{ij} is the overlapping timespan between the two pulsars, χ_{ij} is the overlap reduction function (e.g., the Hellings-Downs correlation function for an isotropic background) that depends on pulsar angular separations (Hellings & Downs 1983; Chamberlain & Siemens 2013), f is the frequency with $f_{\rm L}$ and $f_{\rm H}$ the low- and high-frequency spectral cutoffs, respectively, P_g is the "signal" GW power spectrum¹ ("Earth term"), and $P_{i,j}$ are the total pulsar noise spectra that include the effect of GWs at the pulsar ("pulsar term"). Since power is absorbed by parameter fits in the timing models, we assume a low-frequency cutoff $f_{\rm L}\approx 1/T_{ij}$, due to the spinperiod and spin-period-derivative quadratic subtraction from the TOAs to good approximation (Siemens et al. 2013). Once we compute our individual ρ_{ij} values, the average S/N statistic is given simply by

$$\langle \rho \rangle = \left(\sum \rho_{ij}^2 \right)^{1/2}.$$
 (2)

We will drop the angular brackets denoting the average going forward for brevity.

2.1. Stochastic GW Background

Here we will consider the form of a stochastic GW background of the power-law form (Jenet et al. 2006)

$$P_{\rm SB}(f) = \frac{A_{\rm SB}^2}{12\pi^2} \left(\frac{f}{1\,{\rm yr}^{-1}}\right)^{2\alpha} f^{-3} \equiv bf^{-\beta},$$
 (3)

where $A_{\rm SB}$ is the strain amplitude at a frequency of 1 yr⁻¹ and α is the spectral index of the characteristic strain, where when cast in terms of $\beta = 13/3$ for SMBHBs. Other values exist for primordial GWs or cosmic strings (Jenet et al. 2006). Siemens et al. (2013) provide scaling relations for different regimes of the strength of the signal power spectra versus the

noise power spectra but we consider the full form of the Eq. 1 integral. The pulsar noise spectra are given by three terms,

$$P_i(f) = P_{W,i}(f) + P_{R,i}(f) + P_{SB}(f),$$
 (4)

the sum of the uncorrelated-in-time white noise $P_{\mathrm{W},i}(f)$, correlated-in-time red noise $P_{\mathrm{R},i}(f)$, and time-correlated but spatially-uncorrelated GW pulsar-term with a power spectrum still given by $P_{\mathrm{SB}}(f)$. For a single white-noise rms σ_i , the white-noise term is $P_i(f) = 2\sigma_i^2 \Delta t_i = 2\sigma_i^2/c_i$, where Δt_i is the time between observations and c_i is the equivalent cadence which we use as our per-pulsar model parameter discussed later. Pulsars with red noise were modeled in the form of a power law, $A_{\mathrm{R},i}(f/1\ \mathrm{yr}^{-1})^{-\gamma_i}$, otherwise we assumed $P_{\mathrm{R},i}(f) = 0$. Practically, the white-noise levels change over time due to changes in observing bandwidths, integration times, etc., in which case more generally we have (dropping the subscript i)

$$P_{W,\text{total}}(f) = 2\sigma_{\text{total}}^{2}/c_{\text{total}}$$

$$= 2\sigma_{\text{total}}^{2} \frac{N_{\text{total}}}{T_{\text{total}}}$$

$$= 2\left(\frac{\sum_{n} N_{n} \sigma_{n}^{2}}{\sum_{n} N_{n}}\right) \frac{\sum_{n} N_{n}}{\sum_{n} T_{n}}$$

$$= 2\frac{\sum_{n} (T_{n}/c_{n}) \sigma_{n}^{2}}{\sum_{n} T_{n}}$$

$$= \frac{\sum_{n} P_{W,n}(f) T_{n}}{\sum_{n} T_{n}}$$
(5)

where n denotes different time periods of length T_n , cadence c_n , and rms σ_n , and the number of observations is $N_n = T_n/c_n$.

2.2. Continuous Wave Sources

A common method for CW analyses is to perform searches over a multi-dimensional likelihood function that includes intrinsic source parameters (e.g., chirp mass, GW frequency, strain/distance) along with parameters describing the orientation of the binary with respect to the Earth (Arzoumanian et al. 2014; Babak et al. 2016). Frequentist approaches maximize either an effective matched-filter-type spatially incoherent (\mathcal{F}_p) or coherent statistic $(\mathcal{F}_e;$ Ellis et al. 2012). In the upcoming NG11 analysis of CW sources (K. Aggarwal et al. in prep), we use a Bayesian approach to compute the evidence via a Bayes factor for the parameters while accounting for proper the angular-correlation patterns. We assume here that the correlation must be considered for a detection, as sinusoidal-type waveforms can be present in individual pulsar timing data but due to other systematic effects, such as clock errors or errors in the Solar System ephemerides². Therefore, the *conservative* statistic we maximize over will

¹ We assume one-sided spectra throughout this work.

² In current NANOGrav work, the ephemerides are accounted for using BAYESEPHEM. The errors are expected to be reduced in the future (Arzoumanian et al. 2018b).

take a different form than previous calculations (e.g., the \mathcal{F}_p -statistic).

Using the cross-correlation statistic (Eq. 1), we can again calculate the average S/N but for CWs. Note that we need to modify the equation by replacing χ_{ij} with $\tilde{\chi}_{ij}$, the skylocation-dependent overlap reduction function (Anholm et al. 2009). The signal spectrum for a source with GW frequency $f_{\rm CW}$ is³

$$P_{\rm CW}(f) = \frac{A_{\rm CW}^2}{4\pi^2} \delta_{T_{ij}}(f - f_{\rm CW})f^{-3}, \tag{6}$$

where the approximating function

$$\delta_T(f) \equiv \frac{\sin(\pi f T)}{\pi f} \tag{7}$$

tends to $\delta(f-f_{\rm CW})$ for infinite time and $A_{\rm CW}$ is the amplitude of the GW. Source frequencies are expected to evolve over time such that the pulsars experience lower frequencies than at the Earth (Arzoumanian et al. 2014). Since the signal term (Eq. 6) will cause ρ_{ij} to include power mostly from $f_{\rm CW}$, we do not include $P_{\rm CW}(f)$ in the pulsar noise term though we do include the $P_{\rm SB}(f)$ term.

3. APPLICATION TO THE NANOGRAV 11-YEAR DATA SET

We applied our formalism to the 45 MSPs discussed in NG11. Each pulsar noise model contained several white-noise components and a red-noise power-law model when significant. For simplicity, we used the noise parameters directly reported in the paper (see their Table 2). While work has been done to study the many contributions to the TOA uncertainties (Shannon et al. 2014; Lam et al. 2016), there remain components which have not been well quantified, e.g., from radio-frequency interference or polarization miscalibration (Lam et al. 2018). We took the conservative approach and used the directly measured values from the full timing of each pulsar.

We assumed that during the entire timespan encompassing NG11 each pulsar was observed monthly per year per telescope except for weekly observations of two pulsars at the Green Bank Telescope (GBT) starting in 2013 (PSRs J1713+0747 and J1909–3744 for 30 minutes each) and five pulsars at the Arecibo Observatory (AO) starting in 2015 (PSRs J0030+0451, J1640+2224, J1713+0747, J2043+1711, and J2317+1439 for one hour each); see NG11 for more details. The goal of these observations was to increase the sensitivity of the PTA to CWs (Arzoumanian et al. 2018a). For the high-cadence campaigns, we assumed a time increase of 30 minutes during the non-monthly-observation weeks at GBT or 60 minutes weekly at AO; the total time was 864

hours per year. Recall that the reported white-noise rms of these pulsars will not be affected because we separate out the observational cadence in $P_{W,i}(f)$.

For our optimization analysis, we assumed that the pulsar white-noise rms values were fixed over all epochs, as well as the parameters describing the red-noise power law; future mitigation of timing effects, for example from radio-frequency-dependent pulse-propagation delays, may alter the measured parameters. We note that after the first several years of observing, we switched to wider-bandwidth telescope backends, causing the effective white-noise rms to decrease (see Eq. 5), which we ignore here for simplicity.

For some pulsars where the time baseline was relatively short, the rms noise was very small, largely because the timing-model fit removes more power at longer timescales, e.g., from red noise, than for longer baselines (Blandford et al. 1984; Madison et al. 2013). For example, PSR J2234+0611 was listed with an rms of 30 ns, the lowest of any pulsar yet it was only observed for two years and neither contains the lowest median template-fitting TOA uncertainties (Arzoumanian et al. 2018a) nor does it have the lowest rms from other white-noise sources(M. T. Lam in prep.). Nonetheless, we used all NG11 pulsar noise parameters as reported with the important caveat that future estimates will likely change.

The global-maximum optimization over pulsar cadences was performed using the Nelder-Mead method (Nelder & Mead 1965) implemented in the Python SCIPY package (Gao & Han 2012) via a basin-hopping algorithm (Wales & Doye 1997). To simplify the parameter search, we started with a several-pulsar array and iteratively added pulsars into the array along with the appropriate number of hours per year per source for each telescope, except for PSRs J1713+0747 and B1937+21 where the appropriate time was added to both. We then found the global maximum for that sub-array and used the solution as a starting guess when adding a new pulsar. This algorithm was robust against the order in which pulsars were added. We assumed no new pulsars were to be added to the array and no changes in total observing time from the program at the end of NG11 would be made (both currently untrue). For PSRs J1713+0747 and B1937+21, we assumed for simplicity that they were jitter- and scintillation-noise dominated versus S/N-limited and so the base σ_i was the same at both GBT and AO; this is a good approximation for a majority of observations (Lam et al. 2016; Arzoumanian et al. 2018a) but should be revisited in the future.

We chose three values for the strain amplitude $A_{\rm SB}$ of the SMBHB background: 1×10^{-15} (optimistic), 6×10^{-16} (moderate), and 2×10^{-16} (pessimistic). The most pessimistic lower limit for the background is $\approx 1\times 10^{-16}$ (Dvorkin & Barausse 2017; Bonetti et al. 2018) though most estimates suggest that $A_{\rm SB}$ will be at least several times larger (Ravi et al. 2015). We also looked at two different values of the total timespan observed after the end of NG11, $T_+=10$ or 20 years, for calculating ρ . In Table 1, we show

 $^{^3}$ The boxcar function of length T acts as a finite observing span, which is a multiplication in the Fourier domain of a delta function and normalized sinc function; this procedure can be used to calculate other signal spectra as well. Note the factor of 3 in the denominator versus Eq. 3 from the lack of sky averaging (Anholm et al. 2009; Thrane & Romano 2013)

Table 1. Optimal Pulsar Cadences for a Stochastic Background

| Pulsar | Telescope | Timespan | σ_i | $A_{ m R}$ | γ | Cadence (hours/year) | | | | | | | |
|------------|-----------|----------|------------|------------|-----|---------------------------------------|------------|----------------------------------|----------|----------------------------------|--------------|--|--|
| | | | | | | $A_{\mathrm{SB}} = 1 \times 10^{-15}$ | | $A_{\rm SB} = 6 \times 10^{-16}$ | | $A_{\rm SB} = 2 \times 10^{-16}$ | | | |
| | | (yr) | (μs) | (μs) | | $T_{+} = 10$ | $T_+ = 20$ | $T_{+} = 10$ | $T_+=20$ | $T_{+} = 10$ | $T_{+} = 20$ | | |
| J0023+0923 | AO | 4.4 | 0.308 | _ | _ | 18.9 | 15.6 | 19.3 | 17.8 | 12.7 | 17.4 | | |
| J0030+0451 | AO | 10.9 | 0.241 | 0.025 | 4.0 | 14.0 | 11.6 | 13.3 | 13.4 | 15.2 | 13.1 | | |
| J0340+4130 | GBT | 3.8 | 0.454 | _ | _ | 13.2 | 12.6 | 12.4 | 12.3 | 4.2 | 11.1 | | |
| J0613-0200 | GBT | 10.8 | 0.199 | 0.212 | 1.2 | 9.7 | 8.9 | 11.2 | 9.4 | 15.9 | 11.5 | | |
| J0636+5128 | GBT | 2.0 | 0.611 | _ | _ | 23.0 | 26.3 | 17.7 | 26.2 | _ | 23.7 | | |
| J0645+5158 | GBT | 4.5 | 0.180 | _ | _ | 16.4 | 15.7 | 17.3 | 15.9 | 16.0 | 17.4 | | |
| J0740+6620 | GBT | 2.0 | 0.190 | _ | _ | 17.1 | 15.8 | 17.1 | 15.9 | 10.6 | 17.5 | | |
| J0931-1902 | GBT | 2.8 | 0.495 | _ | _ | 14.9 | 14.5 | 13.9 | 14.3 | _ | 11.6 | | |
| J1012+5307 | GBT | 11.4 | 0.354 | 0.476 | 1.5 | 8.6 | 8.8 | 9.0 | 9.2 | 10.8 | 10.4 | | |
| J1024-0719 | GBT | 6.2 | 0.324 | _ | _ | 12.4 | 11.6 | 13.1 | 11.6 | 11.5 | 12.1 | | |
| J1125+7819 | GBT | 2.0 | 0.483 | _ | _ | 13.5 | 14.8 | 9.9 | 14.6 | _ | 13.0 | | |
| J1453+1902 | AO | 2.4 | 0.757 | _ | _ | _ | 6.7 | _ | 5.7 | _ | _ | | |
| J1455-3330 | GBT | 11.4 | 0.571 | _ | _ | 15.8 | 15.6 | 16.5 | 15.5 | 16.3 | 16.2 | | |
| J1600-3053 | GBT | 8.1 | 0.181 | _ | _ | 16.2 | 15.2 | 18.3 | 15.1 | 26.0 | 17.7 | | |
| J1614-2230 | GBT | 7.2 | 0.183 | _ | _ | 17.8 | 16.5 | 19.6 | 16.7 | 28.2 | 18.9 | | |
| J1640+2224 | AO | 11.1 | 0.382 | _ | _ | 16.7 | 13.5 | 16.4 | 14.6 | 18.0 | 14.5 | | |
| J1643-1224 | GBT | 11.2 | 0.757 | 1.619 | 1.3 | 11.2 | 11.2 | 11.8 | 11.9 | 10.8 | 12.4 | | |
| J1713+0747 | AO/GBT | 10.9 | 0.103 | 0.021 | 1.6 | 14.1/9.3 | 13.6/8.6 | 15.9/10.5 | 14.8/8.7 | 22.3/16.4 | 15.2/10.5 | | |
| J1738+0333 | AO | 6.1 | 0.364 | _ | _ | 26.4 | 24.5 | 27.2 | 24.7 | 29.0 | 26.3 | | |
| J1741+1351 | AO | 6.4 | 0.102 | _ | _ | 20.6 | 20.2 | 22.4 | 19.7 | 29.8 | 21.4 | | |
| J1744-1134 | GBT | 11.4 | 0.403 | _ | _ | 21.6 | 21.4 | 23.5 | 21.7 | 29.8 | 23.2 | | |
| J1747-4036 | GBT | 3.8 | 1.580 | 1.823 | 1.4 | 7.4 | 14.0 | _ | 12.0 | _ | _ | | |
| J1832-0836 | GBT | 2.8 | 0.184 | _ | _ | 21.5 | 19.6 | 23.5 | 19.9 | 30.9 | 22.7 | | |
| J1853+1303 | AO | 4.5 | 0.205 | _ | _ | 35.1 | 35.5 | 36.9 | 35.4 | 45.2 | 38.4 | | |
| B1855+09 | AO | 11.0 | 0.482 | 0.069 | 3.0 | 29.1 | 31.4 | 28.1 | 29.6 | 26.9 | 30.3 | | |
| J1903+0327 | AO | 6.1 | 0.573 | 1.615 | 2.1 | 18.4 | 19.4 | 20.2 | 22.9 | 17.1 | 24.9 | | |
| J1909-3744 | GBT | 11.2 | 0.070 | 0.042 | 1.7 | 7.3 | 6.7 | 8.1 | 6.8 | 11.5 | 8.2 | | |
| J1910+1256 | AO | 6.8 | 0.515 | _ | _ | 37.7 | 36.5 | 34.3 | 36.0 | 28.7 | 35.3 | | |
| J1911+1347 | AO | 2.4 | 0.054 | _ | _ | 21.2 | 20.9 | 23.6 | 20.7 | 32.6 | 23.1 | | |
| J1918-0642 | GBT | 11.2 | 0.297 | _ | _ | 19.4 | 19.3 | 21.3 | 19.3 | 28.7 | 21.4 | | |
| J1923+2515 | AO | 4.3 | 0.229 | _ | _ | 35.0 | 33.7 | 36.3 | 32.9 | 38.3 | 35.4 | | |
| B1937+21 | AO/GBT | 11.3 | 0.110 | 0.157 | 2.8 | 8.1/19.7 | 7.5/20.7 | 9.2/21.8 | 7.7/20.5 | 13.8/29.7 | 9.2/23.7 | | |
| J1944+0907 | AO | 4.4 | 0.333 | _ | _ | 35.7 | 35.9 | 38.2 | 37.4 | 35.6 | 38.5 | | |
| B1953+29 | AO | 4.4 | 0.394 | _ | _ | 32.4 | 33.1 | 32.3 | 32.5 | 27.6 | 31.7 | | |
| J2010-1323 | GBT | 6.2 | 0.260 | _ | _ | 17.5 | 16.2 | 19.5 | 16.4 | 25.1 | 18.6 | | |
| J2017+0603 | AO | 3.8 | 0.091 | _ | _ | 24.7 | 25.1 | 26.1 | 24.8 | 34.7 | 24.6 | | |
| J2033+1734 | AO | 2.3 | 0.500 | _ | _ | 38.1 | 39.4 | 34.0 | 38.4 | _ | 38.1 | | |
| J2043+1711 | AO | 4.5 | 0.119 | _ | _ | 26.0 | 26.0 | 28.3 | 25.1 | 36.0 | 27.2 | | |
| J2145-0750 | GBT | 11.3 | 0.304 | 0.589 | 1.3 | 6.4 | 5.9 | 7.2 | 6.3 | 9.2 | 7.8 | | |
| J2214+3000 | AO | 4.2 | 1.330 | _ | _ | 9.3 | 17.4 | _ | 14.0 | _ | _ | | |
| J2229+2643 | AO | 2.4 | 0.203 | _ | _ | 20.9 | 18.6 | 20.9 | 18.7 | 15.1 | 18.1 | | |
| J2234+0611 | AO | 2.0 | 0.030 | _ | _ | 8.6 | 7.0 | 8.1 | 7.1 | 11.8 | 8.3 | | |
| J2234+0944 | AO | 2.5 | 0.205 | _ | _ | 26.9 | 23.2 | 26.9 | 23.4 | 25.5 | 24.4 | | |
| J2302+4442 | GBT | 3.8 | 0.836 | _ | _ | 7.8 | 9.3 | 4.5 | 8.3 | _ | _ | | |
| J2317+1439 | AO | 11.0 | 0.287 | _ | _ | 18.3 | 18.4 | 17.4 | 17.8 | 16.4 | 17.9 | | |

We assumed $\beta=13/3$. Added timespan T_+ is in units of years. Dashed entries formally have values but are too small to be reported.

 Table 2. Optimal Pulsar Cadences for Continuous Wave Sources

| Pulsar | Telescope | Timespan | σ_i | A_{R} | γ | Cadence (hours/year) | | | | | |
|--------------|-----------|----------|------------|------------------|----------|----------------------|-----------|-----------|----------|-----------|--|
| | | (yr) | (μs) | (μs) | | M84 | M104 | NGC 3115 | NGC 1316 | All Sky | |
| J0023+0923 | AO | 4.4 | 0.308 | _ | _ | _ | _ | _ | 26.6 | _ | |
| J0030+0451 | AO | 10.9 | 0.241 | 0.025 | 4.0 | _ | _ | _ | 29.5 | 1.3 | |
| J0340+4130 | GBT | 3.8 | 0.454 | _ | _ | _ | _ | _ | 2.1 | _ | |
| J0613-0200 | GBT | 10.8 | 0.199 | 0.212 | 1.2 | _ | 1.9 | 5.7 | 8.8 | 1.4 | |
| J0636+5128 | GBT | 2.0 | 0.611 | _ | _ | _ | _ | _ | _ | _ | |
| J0645+5158 | GBT | 4.5 | 0.180 | _ | _ | 55.6 | 14.8 | 74.7 | 76.6 | 20.5 | |
| J0740+6620 | GBT | 2.0 | 0.190 | _ | _ | 81.7 | _ | 120.9 | 56.4 | 30.2 | |
| J0931 - 1902 | GBT | 2.8 | 0.495 | _ | _ | 1.1 | _ | _ | 13.3 | _ | |
| J1012+5307 | GBT | 11.4 | 0.354 | 0.476 | 1.5 | 1.9 | _ | 2.5 | _ | _ | |
| J1024-0719 | GBT | 6.2 | 0.324 | _ | _ | 35.7 | 37.5 | 59.1 | 15.5 | 2.8 | |
| J1125+7819 | GBT | 2.0 | 0.483 | _ | _ | _ | _ | _ | _ | _ | |
| J1453+1902 | AO | 2.4 | 0.757 | _ | _ | _ | _ | 60.0 | _ | _ | |
| J1455-3330 | GBT | 11.4 | 0.571 | _ | _ | _ | 5.0 | _ | _ | _ | |
| J1600-3053 | GBT | 8.1 | 0.181 | _ | _ | 40.8 | 57.5 | _ | 16.8 | 32.5 | |
| J1614-2230 | GBT | 7.2 | 0.183 | _ | _ | 36.5 | 66.5 | 5.1 | 13.8 | 36.7 | |
| J1640+2224 | AO | 11.1 | 0.382 | _ | _ | 20.8 | 6.6 | 34.1 | _ | _ | |
| J1643-1224 | GBT | 11.2 | 0.757 | 1.619 | 1.3 | _ | _ | _ | _ | _ | |
| J1713+0747 | AO/GBT | 10.9 | 0.103 | 0.021 | 1.6 | 69.2/28.6 | 82.4/30.2 | 99.5/35.3 | -/9.0 | 30.2/48.1 | |
| J1738+0333 | AO | 6.1 | 0.364 | _ | _ | 6.1 | 19.6 | 34.0 | _ | _ | |
| J1741+1351 | AO | 6.4 | 0.102 | _ | _ | 116.5 | 119.5 | 141.4 | _ | 51.3 | |
| J1744-1134 | GBT | 11.4 | 0.403 | _ | _ | _ | 6.5 | _ | _ | 6.8 | |
| J1747-4036 | GBT | 3.8 | 1.580 | 1.823 | 1.4 | _ | _ | _ | _ | _ | |
| J1832-0836 | GBT | 2.8 | 0.184 | _ | _ | 9.7 | 59.3 | _ | 38.4 | 60.8 | |
| J1853+1303 | AO | 4.5 | 0.205 | _ | _ | 49.5 | 43.0 | 39.7 | _ | 25.4 | |
| B1855+09 | AO | 11.0 | 0.482 | 0.069 | 3.0 | _ | _ | _ | _ | _ | |
| J1903+0327 | AO | 6.1 | 0.573 | 1.615 | 2.1 | _ | _ | _ | _ | _ | |
| J1909-3744 | GBT | 11.2 | 0.070 | 0.042 | 1.7 | 16.4 | 26.8 | 12.0 | 41.6 | 32.3 | |
| J1910+1256 | AO | 6.8 | 0.515 | _ | _ | _ | _ | _ | _ | _ | |
| J1911+1347 | AO | 2.4 | 0.054 | _ | _ | 146.2 | 148.8 | 134.6 | 50.6 | 123.4 | |
| J1918-0642 | GBT | 11.2 | 0.297 | _ | _ | _ | 4.5 | _ | 4.5 | 13.8 | |
| J1923+2515 | AO | 4.3 | 0.229 | _ | _ | 22.8 | 15.6 | _ | _ | 13.3 | |
| B1937+21 | AO/GBT | 11.3 | 0.110 | 0.157 | 2.8 | 6.6/7.0 | 3.7/8.5 | -/4.5 | 2.9/3.3 | 11.4/8.2 | |
| J1944+0907 | AO | 4.4 | 0.333 | _ | _ | _ | _ | _ | _ | _ | |
| B1953+29 | AO | 4.4 | 0.394 | _ | _ | _ | _ | _ | _ | _ | |
| J2010-1323 | GBT | 6.2 | 0.260 | _ | _ | _ | 1.7 | _ | 15.3 | 17.7 | |
| J2017+0603 | AO | 3.8 | 0.091 | _ | _ | 70.1 | 68.6 | _ | 72.3 | 74.9 | |
| J2033+1734 | AO | 2.3 | 0.500 | _ | _ | _ | _ | _ | _ | _ | |
| J2043+1711 | AO | 4.5 | 0.119 | _ | _ | 29.3 | 29.8 | _ | 66.8 | 61.1 | |
| J2145-0750 | GBT | 11.3 | 0.304 | 0.589 | 1.3 | _ | _ | _ | _ | _ | |
| J2214+3000 | AO | 4.2 | 1.330 | _ | _ | _ | _ | _ | _ | _ | |
| J2229+2643 | AO | 2.4 | 0.203 | _ | _ | _ | _ | _ | 59.6 | 20.1 | |
| J2234+0611 | AO | 2.0 | 0.030 | _ | _ | 10.4 | 5.5 | _ | 107.1 | 89.5 | |
| J2234+0944 | AO | 2.5 | 0.205 | _ | _ | _ | _ | _ | 112.1 | 45.0 | |
| J2302+4442 | GBT | 3.8 | 0.836 | _ | _ | _ | _ | _ | _ | _ | |
| J2317+1439 | AO | 11.0 | 0.287 | _ | _ | _ | _ | _ | 19.3 | 4.1 | |

We assumed $A_{\rm CW}=1\times 10^{-15},\,f_{\rm CW}=0.5{\rm yr}^{-1},\,A_{\rm SB}=1\times 10^{-15},$ and $T_+=20$ years. Dashed entries formally have values but are too small to be reported.

our results in terms of the amount of time per pulsar per year allocated given different values of $A_{\rm SB}$ and T_+ .

3.1. Maintaining the PTA: The Time Allocation Per Pulsar

Table 1 shows that our best pulsars do not overwhelmingly dominate the stochastic-background time allocation. This makes sense when we consider a hypothetical PTA where we ignore all T_{ij} and χ_{ij} and only have pulsars with white noise. Following Siemens et al. (2013) but including the differences in white noise and cadences, we have $\rho_{ij} \propto [(c_i c_j)/(\sigma_i^2 \sigma_j^2)]^{1/2}$. Then, one can easily show that the total ρ maximizes when the "quality" of each pulsar, the white-noise spectrum $2\sigma_i^2/c_i$, is similar, and thus one should spend more time on pulsars with higher white-noise rms. For real PTAs, one should consider red noise, varying time baselines, and sky positions, which will modify the results accordingly though the basic principle still applies. We see that the time allocation is of similar magnitude for all pulsars, though several pulsars do not contribute significantly for certain assumed parameters and thus are not listed (when $c_i < 1$ hour/year).

Comparing against a continuation of the NG11 observing strategy versus the optimizations found here, we see a ${\sim}5\%$ increase in ρ for $A_{\rm SB}=1\times10^{-15}$ but a nearly $\sim8-10\%$ increase for $A_{\rm SB}=2\times10^{-16}$. NANOGrav's general strategy of observing many high-precision pulsars with roughly equal time (along with high-cadence programs) therefore currently provides close to optimal stochastic-background sensitivity.

3.2. Trimming the PTA: Removing Pulsars to Improve Sensitivity

Figure 1 shows the effect of removing a pulsar from the array and whether reallocating its observing time will increase or decrease sensitivity to the stochastic background. We find that all 45 pulsars contribute significantly for decadeslong experiments and that the relative importance of continuing to time these pulsars also tends to improve. However, note in Table 1 where certain pulsars become significant for $T_+=20$ years whereas they are unlisted for earlier times. Formally we find values for these pulsars though they are too small to report given the practical necessity of requiring enough observations to generate a timing solution. The *GW significance seems robust to red noise*, as for PSR J0030+0451 the red-noise index $\gamma=4.0$, which is steeper than the background $\beta=13/3$.

3.3. Directional PTA Tuning

For CW sources, we looked at specific potential galaxies that may host SMBHBs. Mingarelli et al. (2017) examined the detectability of individual local SMBHBs by simulating binaries within nearby host galaxies; they estimated that a single source will likely be detectable within ~10 years from now. Assuming different noise statistics of pulsars observed by the International Pulsar Timing Array (IPTA; Verbiest et al. 2016), different potential sources may be detectable. Assuming only white noise in the IPTA pulsars, they found that M104 (NGC 4594) may likely host a detectable CW

source. In a more updated analysis, they find that M104 is the most likely detectable SMBHB source regardless of the assumed black-hole/galaxy-host scaling relation, followed consistently by M84 (NGC 4374; C. Mingarelli, private communication). NGCs 3115 and 1316 also feature prominently as possible SMBHB-host candidates regardless of pulsar rednoise properties. We looked at these four specific sources independently, shown for reference in Figure 2, and assumed $T_+=20$ years, a source strain of $A_{\rm CW}=10^{-15}$ and frequency $f_{\rm CW}=0.5~{\rm yr}^{-1}$, and a stochastic-background pulsar term of $A_{\rm SB}=10^{-15}$. For comparison, we also considered sources uniformly distributed across the sky with the same assumed parameters and maximized the S/N over all sky positions θ_n as

$$\rho_{\text{sky}} = \left(\sum_{n} \left[\rho(\boldsymbol{\theta}_n)\right]^2\right)^{1/2}.$$
 (8)

The results of our CW analysis are given in Table 2. We find that many pulsars contribute to the sensitivity towards different sources though typically different pulsars are pre*ferred*; this differs from an analysis using the \mathcal{F}_p -statistic without sky correlations included in which one or two pulsars dominate the S/N (Arzoumanian et al. 2014; Babak et al. 2016). Tests using lower $f_{\rm CW}$ show a preference for a greater number of pulsars with similar c_i , i.e., these sources suggest an observing program more similar to the stochastic background. Recall that the ρ statistic is conservative since it includes correlations but sub-optimal since it does not include signal-waveform matched-filtering. Again, note the caveats above on the uncertainty in the pulsar noise properties, which is why PSRs J1911+1347 and J2234+0611 contribute significantly in the all-sky analysis. Since M104 and M84 are $\sim 25^{\circ}$ separated on the sky, and both $\sim 40^{\circ}$ from NGC 3115, we see significant overlap for the pulsars that contribute to ρ . For these sources, PSRs J1744-1134 and J1918-0642 take up significant portions of observing time in part due to the long timespans and strong correlations with PSR J1713+0747.

It is possible to "tune" PTA observations to efficiently improve the S/N towards multiple targets. In general one can construct a metric that maximizes the sensitivity to a number of possible sources across the sky, potentially in a form similar to Eq. 8, and likely should given that any one individual galaxy hosts a detectable CW source is not guaranteed. Current and future PTA experiments may wish to increase their sensitivity to specific sky locations in order to hasten a detection and also improve later characterization, for example in studying the galaxy members of the nearby Virgo cluster in addition to the sources analyzed here.

4. FUTURE APPLICATIONS

We briefly discuss several next steps for improving GW sensitivity via this framework. One obvious next step is to determine methods of combining the metric provided here that is some weighted combination of different ρ statistics for a stochastic background and specific CW sources, though as

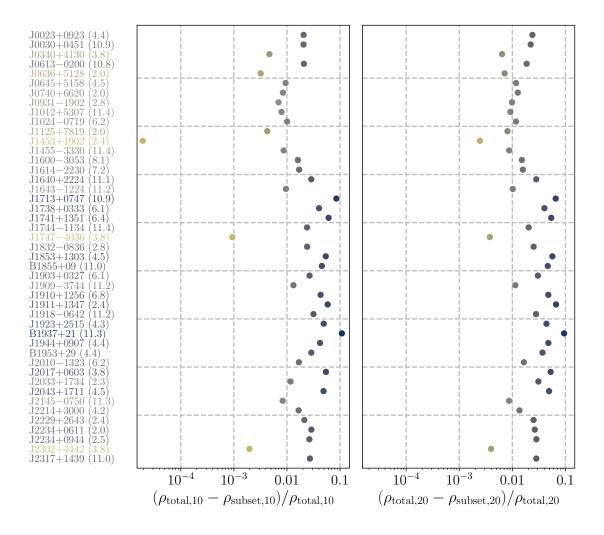


Figure 1. The metric $(\rho_{\text{total}} - \rho_{\text{subset}})/\rho_{\text{total}}$ shows the fractional difference between the S/N of the whole PTA ρ_{total} and the S/N when the pulsar listed is removed and the time is reallocated and reoptimized ρ_{subset} . The larger the metric, the more important the individual pulsar is in contributing to the PTA's GW sensitivity. Here we assume $A_{\text{SB}} = 1 \times 10^{-15}$. The left panel shows the metric per pulsar when observing for an additional $T_{+} = 10$ years, the right panel for an additional $T_{+} = 20$ years. The total time observed for each pulsar in NG11 is shown in the parentheses (in years). The colors of the pulsar names are the same as of the point in the left panel, which is correlated with the metric.

various project science goals may differ, we will not expand further.

4.1. Obtaining Robust Noise Parameters

As mentioned previously, our results for specific pulsars are skewed because some pulsars with short time baselines have very small rms values. Since the red-noise rms grows with time, it may take many years before a full noise profile is obtained for a given pulsar. Therefore, one can either make a predictive guess of how well a pulsar will perform using various models for red noise (e.g., Lam et al. 2017, note that there is large scatter in scalings for intrinsic-spin or interstellar-medium-related noise) or a postdictive recalculation of the different metrics presented here in an attempt to optimize future GW sensitivity.

4.2. Implementation of Wideband Receivers

While NANOGrav currently observes one pulsar per hour per telescope per epoch, it does so by splitting each observation into two half-hour segments for each frequency receiver. Therefore, 60 minutes of observing time (including overhead) equates to $\lesssim 30$ minutes of effective integration time. Wideband receivers will allow for a doubling of the effective integration time for the same on-sky time; in practice a wideband receiver will have a somewhat higher system temperature and an optimization for the best frequency tuning should be performed for maximizing TOA precision (Lam et al. 2018). While our framework applies generally, with different observational parameters we expect the results of our analyses to differ and one should account for as many inputs as possible in developing observing strategies.

4.3. International Pulsar Timing Array

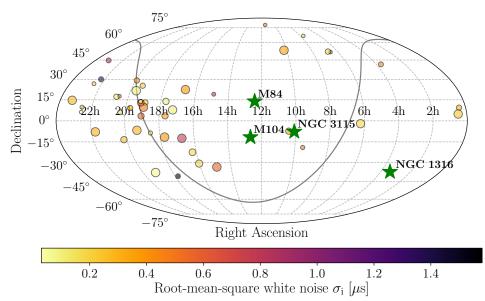


Figure 2. Sky positions of our pulsars (circles) in relation to the four CW sources (stars). Circles sizes are proportional to the timespan observed T_i , the colors are proportional to the white-noise rms σ_i . The curve denotes the Galactic plane.

Different PTA collaborations pool their resources into the IPTA collaboration. Each member currently has separate observing strategies. With the resources of many radio telescopes, the best possible GW sensitivity will be obtained by performing the optimization we have laid out across the combined network. Given the differing sensitivities, radio frequency coverages, and cadences of the telescopes, along with practical constraints, it may be preferential for individual telescopes to observe different sources rather than multiple

telescopes spending their time to observe the same sources. Future analyses must be performed to investigate how best to optimize all of the IPTA telescopes, especially as new potential member collaborations seek to join.

Acknowledgments. We graciously thank Xavier Siemens, Maura McLaughlin, Stephen Taylor, and Chiara Mingarelli for discussions enabling this work. M.T.L. and the NANOGrav Project receives support from NSF Physics Frontiers Center award number 1430284.

REFERENCES

Anholm, M., Ballmer, S., Creighton, J. D. E., Price, L. R., & Siemens, X. 2009, PhRvD, 79, 084030

Arzoumanian, Z., Brazier, A., Burke-Spolaor, S., et al. 2014, ApJ, 794, 141

Arzoumanian, Z., Brazier, A., Burke-Spolaor, S., et al. 2015a, ApJ, 810, 150

Arzoumanian, Z., Brazier, A., Burke-Spolaor, S., et al. 2015b, ApJ, 813, 65

Arzoumanian, Z., Brazier, A., Burke-Spolaor, S., et al. 2018a, ApJS, 235, 37

Arzoumanian, Z., Baker, P. T., Brazier, A., et al. 2018b, ApJ, 859, 47

Babak, S., Petiteau, A., Sesana, A., et al. 2016, MNRAS, 455, 1665Blandford, R., Narayan, R., & Romani, R. W. 1984, Journal of Astrophysics and Astronomy, 5, 369

Bonetti, M., Sesana, A., Barausse, E., & Haardt, F. 2018, MNRAS, 477, 2599

Chamberlain, S. J., & Siemens, X. 2012, Phys. Rev. D 85, 082001

Cornish, N. J., & Sesana, A. 2013, Classical and Quantum Gravity, 30, 224005

Desvignes, G., Caballero, R. N., Lentati, L., et al. 2016, MNRAS, 458, 3341

Dvorkin, I., & Barausse, E. 2017, MNRAS, 470, 4547

Ellis, J. A., Siemens, X., & Creighton, J. D. E. 2012, ApJ, 756, 175

Gao, F. & Han, L. 2012, Computational Optimization and Applications, 51, 259

Hellings, R. W., & Downs, G. S. 1983, ApJL, 265, L39

Jenet, F. A., Hobbs, G. B., van Straten, W., et al. 2006, ApJ, 653, 1571

Lam, M. T., Cordes, J. M., Chatterjee, S., et al. 2016, ApJ, 819, 155

Lam, M. T., Cordes, J. M., Chatterjee, S., et al. 2017, ApJ, 834, 35

Lam, M. T., McLaughlin, M. A., Cordes, J. M., Chatterjee, S., & Lazio, T. J. W. 2018, ApJ, 861, 12

Lee, K. J., Bassa, C. G., Janssen, G. H., et al. 2012, MNRAS, 423, 2642

Madison, D. R., Chatterjee, S., & Cordes, J. M. 2013, ApJ, 777, 104

- McLaughlin, M. A. 2013, Classical and Quantum Gravity, 30, 224008
- Mingarelli, C. M. F., Lazio, T. J. W., Sesana, A., et al. 2017, Nature Astronomy, 1, 886
- Nelder, J. A., & Mead R. 1965, The Computer Journal, 7, 4, 308Ravi, V., Wyithe, J. S. B., Shannon, R. M., & Hobbs, G. 2015,MNRAS, 447, 2772
- Reardon, D. J., Hobbs, G., Coles, W., et al. 2016, MNRAS, 455, 1751
- Siemens, X., Ellis, J., Jenet, F., & Romano, J. D. 2013, Classical and Quantum Gravity, 30, 224015

- Shannon, R. M., Osłowski, S., Dai, S., et al. 2014, MNRAS, 443, 1463
- Taylor, S. R., Vallisneri, M., Ellis, J. A., et al. 2016, ApJL, 819, L6 Thrane, E., & Romano, J. D. 2013, PhRvD, 88, 124032
- Verbiest, J. P. W., Lentati, L., Hobbs, G., et al. 2016, MNRAS, 458, 1267
- Vigeland, S. J., & Siemens, X. 2016, PhRvD, 94, 123003
- Vitale, S., Cerdonio, M., Coccia, E., & Ortolan, A. 1997, PhRvD, 55, 1741
- Wales, D. J., & Doye J. P. K. 1997, Journal of Physical Chemistry A, 101, 5111